Propellant Loading Effects on Ferroelectric Plasma Thruster Performance and Possible Applications

IEPC-2009-177

Presented at the 31st International Electric Propulsion Conference,
University of Michigan • Ann Arbor, Michigan • USA
September 20 – 24, 2009

Brian T. Hutsel[1], Scott D. Kovaleski[2] and Craig Kluever[3]
University of Missouri, Columbia, MO, 65211, USA

Abstract: A ferroelectric plasma thruster (FEPT) is being developed for propulsion of microspacecraft. This paper further details experiments completed on the effects of surface materials used as propellant on FEPT performance. Additionally an analysis of a potential on-orbit application for FEPT's is performed.

I. Introduction

MICROSPACECRAFT require a propulsion mechanism with a high specific impulse, low weight, and high efficiency [1]. Ferroelectric plasma thrusters (FEPTs) are being developed for microspacecraft propulsion applications. The FEPT requires a single RF power supply, utilizes no liquid propellants, and has the potential to be self-neutralizing. These advantages lead a low weight propulsion mechanism allowing for high specific impulses.

FEPTs utilize ion and electron emission from an RF driven ferroelectric to provide propulsion. A diagram and photograph of the FEPT is shown in Fig. 1. Emission from the FEPT is similar to ferroelectric emission (FEE) cathodes [2,3] and ferroelectric plasma sources (FPSs), relying on triple point emission followed by surface plasma extraction [4,5]. The RF power supply produces thrust by accelerating the ions and electrons via a ponderomotive-like force [6].

Proof of concept studies and initial measurements of the operating characteristics have previously been completed for one operating setpoint of the FEPT [7]. Table 1 details the initial thruster characteristics. In order to produce a space-ready device, further optimization of FEPT performance is necessary. The University of Missouri is investigating the effects of additional solid materials placed on the surface of the ferroelectric in the aperture of

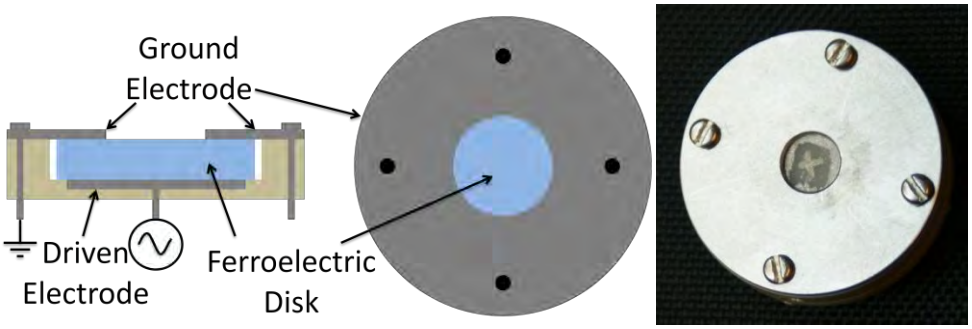

Figure 1. FEPT diagram and image. (a) cross-section view (b) top view of ground electrode and aperture (c) image of FEPT.

[1] Graduate Research Assistant, Electrical and Computer Engineering, bthwtb@mail.mizzou.edu.
[2] Associate Professor, Electrical and Computer Engineering, kovaleskiS@missouri.edu
[3] Professor, Mechanical and Aerospace Engineering, KlueverC@missouri.edu.

the FEPT on the ion and electron emission from the device. Additionally, an analysis of a potential on-orbrit application for FEPTs is performed.

TABLE 1
FEPT THRUSTER CHARACTERISTICS [7]

Thrust	68-87 μN
Specific Impulse	600 s
Average Power	6 W
Impulse Bit	< 1 nN*s
Thrust efficiency	8%

II. Propellant loading

The ion beam produced by the FEPT is composed of the surface materials present in the aperture of the thruster [8]. These materials consist of lithium and niobium, from the ferroelectric, and silver, used to electrode the ferroelectric. One important parameter that was examined was the use of additional solid materials deposited in the FEPT aperture. The ablation and acceleration of the additional material serve as the mass transfer mechanism for the thruster to produce thrust.

A. Experiment Setup

To add additional materials to the surface, varying amounts of silver paint were applied in the aperture of the FEPT. Images of the varying electrode geometries are shown in Fig. 2. The ground electrode is seen on the outside of the disk. The additional material can be seen in samples (b) and (c) in the center of the disk. To quantify the amount of material added, the mass of the ferroelectric disk was measured before and after applying the additional silver paint using an Ohaus DV215CD microbalance. A summary of the samples used in the experiment are shown in Table 2. Included is a description of the geometry of the added material and the mass of silver paint added to the surface

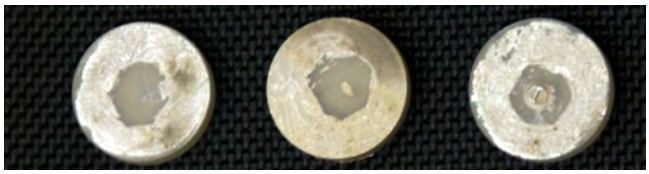

(a) (b) (c)

Figure 2. Sample images of some of the FEPT configurations tested. (a) no added surface material in aperture. (b) small amount of added surface material . (c) large amount of added surface material.

TABLE 2
FEPT CONFIGURATIONS TESTED

Disk	Description	Mass Added
A	No added mass	0 μg
B	Small added mass in center	590 μg
C	Large added mass in center	1390 μg
D	Mass added in "x" shape	200 μg

To measure the effect of the additional materials, the emitted electron and ion currents were measured using a Faraday cup and a 1 kΩ current viewing resistor (CVR). The FEPT was operated in vacuum with pressure of 6 to 10 μtorr.

B. Results

Emission from the crystals varied based on the amount of silver paint applied as solid propellant. Electron emission was observed in all samples, however ion emission was only observed in samples with added silver paint. Fig. 3 is a comparison of a FEPT with and without additional solid propellant. Emission current from disk A shows only electron emission during the negative half-cycle of applied voltage. Fig. 3b shows both electron emission during the negative half-cycle and ion emission during the positive half-cycle for disk C with 1390 µg of applied silver paint as solid propellant.

Additionally, it was observed that the ion emission was of greater intensity and frequency as more silver paint was added. Fig. 4 compares the current emission of an FEPT with 200 µg and 1390 µg of silver paint. The total ion charge emitted from the 200 µg disk over the 38 cycles shown in Fig. 4a was 20.4 nC corresponding to an average ion current of 0.2 mA. Disk C, with 1390 µg of added propellant, emitted a total ion charge of 118.8 nC over 38 cycles with an average ion current of 1.18 mA.

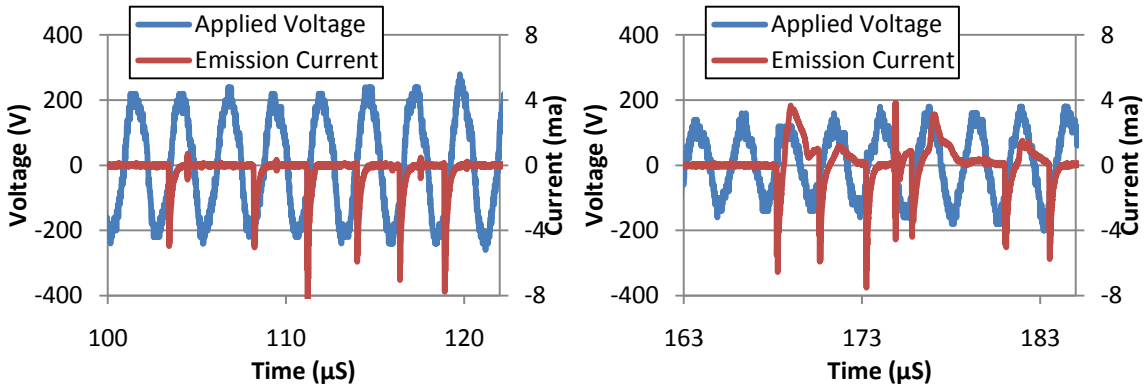

(a) (b)

Figure 3. Measured electron and ion current emitted from (a) Disk A (b) Disk C (from Table 2). No ion emission was measured from Disk A which contained no additional silver paint.

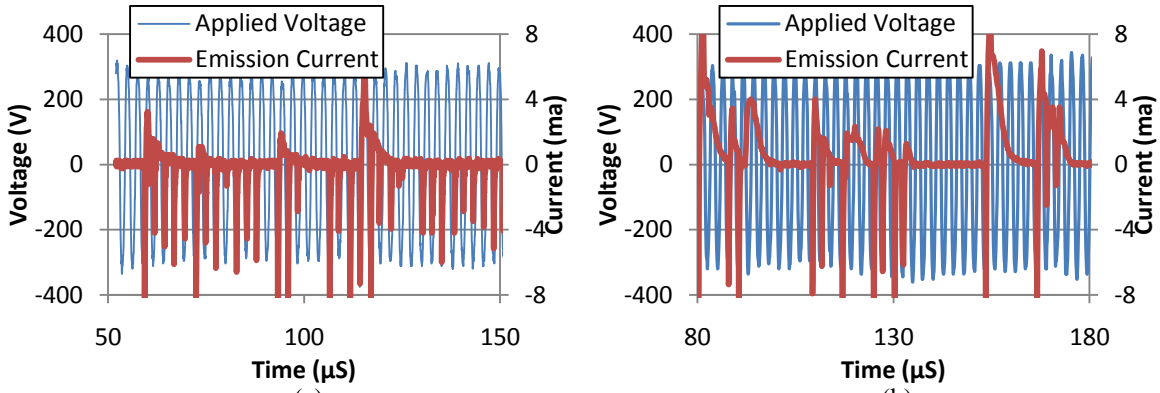

(a) (b)

Figure 4. Measured ion and electron current emitted from (a) Disk D and (b) Disk C (from Table 2). Measured ion emission was more frequent and greater magnitude from a crystal with more applied silver paint.

III. On-Orbit Application Analysis

A. Stationkeeping and Drag Compensation

Stationkeeping involves performing relatively small orbital corrections using propulsive maneuvers in order to maintain a desired orbit. Atmospheric drag is a dominate perturbation for satellites in low-Earth orbit (LEO). Drag

affects the attitude (angular orientation) of the satellite, as well as the size, shape, and orientation of the orbit. The fundamental equation for drag force D is

$$D = \frac{1}{2}\rho V_{rel}^2 S C_D \tag{1}$$

where ρ is atmospheric density, V_{rel} is the speed of the satellite relative to the atmosphere, S is the reference area for the satellite, and C_D is the drag coefficient. By definition, the drag force is always aligned anti-parallel to the satellite's velocity vector, and therefore drag continually reduces the orbital energy. Satellites in LEO will eventually re-enter the Earth's atmosphere due to the long-term cumulative effect of drag unless a propulsive force is periodically applied to re-boost the orbit. As an example, drag will cause the semi-major axis to decrease by 5 km/day for a 200-km altitude LEO.

In order to demonstrate the potential application of FEPT for drag compensation, we will estimate the first-order effects of drag for three classes of miniature satellites: 1) micro-satellites (total mass 10-100 kg), 2) nano-satellites (1-10 kg), and 3) pico-satellites (0.1-1 kg). We will base our micro-satellite characteristics on the XS-11, which was developed by the U.S. Air Force Research Laboratory to test technology for proximity operations [9]. Our nano-satellite characteristics are based on the Miniature Autonomous Extravehicular Robotic Camera (Mini AERCam), which is a proposed free-flying viewing system that could be used to provide damage inspection of the International Space Station [10]. Our pico-satellite characteristics are based on CubeSat, which was developed by a team of university students and professors, primarily from California Polytechnic State University and Stanford University [11]. Table 3 summarizes the characteristics of these three satellites, including mass, area, drag coefficient, and ballistic coefficient $\beta = m/(S C_D)$.

TABLE 3
CHARACTERISTICS OF MINIATURE SATELLITES USED IN NUMERICAL TRIALS

Satellite class	Wet mass, m (kg)	Reference area, S (m^2)	Drag coefficient, C_D	Ballistic coefficient, β (kg/m^2)
Pico-satellite	1	0.01	1.8 (plate)	55.6
Nano-satellite	5	0.0285	1.0 (sphere)	175.4
Micro-satellite	100	1.000	1.8 (plate)	55.6

Orbital velocity varies with altitude, and upper atmospheric density ρ is computed by using the Harris-Priester model which includes the averaged effects due to solar cycle fluxes and seasonal latitude variations [12]. Our single FEPT was modeled with specific impulse I_{sp} = 600 sec, efficiency of 8%, and thrust magnitude of 68 μN. The mass of one FEPT is 5.7 g (0.0057 kg).

The required number of FEPTs for drag compensation can be computed by dividing the drag force (at the respective altitude) by the thrust of a single FEPT (i.e., 68 μN). The drag force is multiplied by a factor of 3 in order to approximate a "duty cycle" where the thrusters only fire for segments of an orbital arc (perhaps two 45-deg arcs, centered near perigee and apogee), or a drag-compensation burn over an entire orbital revolution after 3 coasting orbital revolutions. The number of required thrusters is rounded up to the highest integer. Fig. 5 shows the total number of required FEPTs for drag compensation. Clearly, as LEO altitude is lowered, the number of FEPTs increases dramatically. However, for altitudes above 200 km, the number of FEPTs required for drag make-up is less than 10 for the pico- and nano-satellite classes, which is a feasible propulsion option. Fig. 6 presents the total power required for the array of FEPTs. Power P for a single FEPT is computed using

$$P = \frac{TgI_{sp}}{2\eta} \tag{2}$$

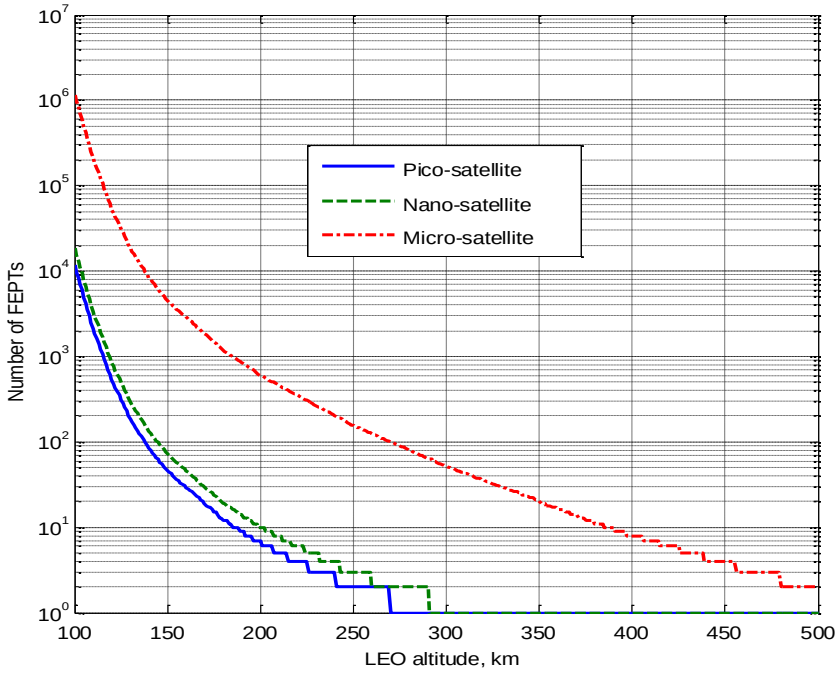

Figure 5. Number of FEPTs required for drag compensation.

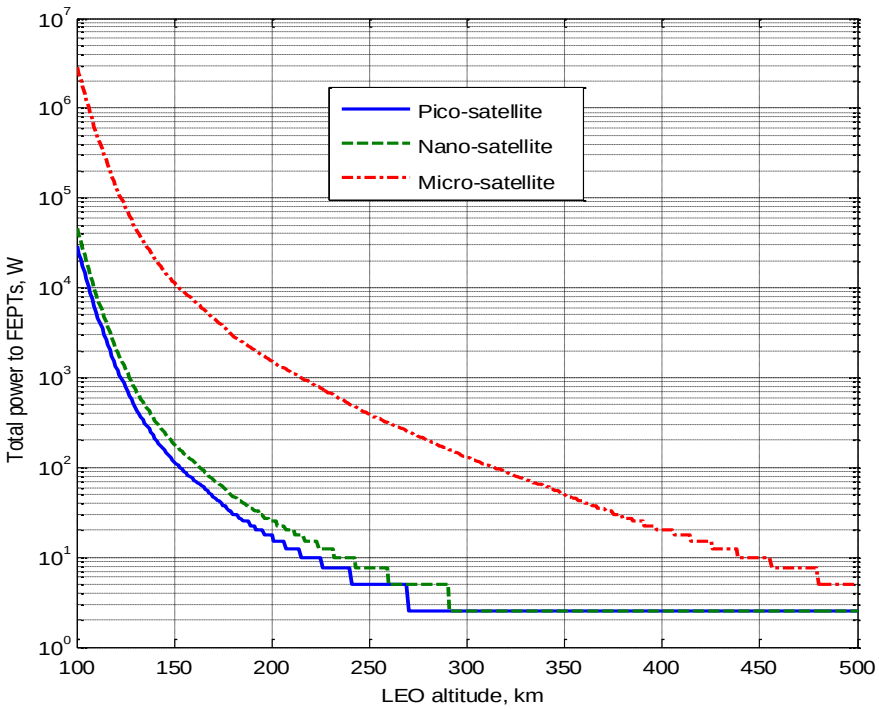

Figure 6. Total input power to FEPTs required for drag compensation.

Therefore, input power for a single FEPT is 2.5 W. Total input power is computed by multiplying the number of FEPTs (Fig. 5) by 2.5 W, and Fig. 6 shows that total input power drops below 30 W for the pico- and nano-satellites when altitude is above 200 km. The input power required for a micro-satellite drops below 100 W when LEO altitude is above 320 km.

Fig. 7 shows the FEPT engine mass fraction, or ratio of total FEPT mass divided by the initial (wet) mass. It is interesting that the pico- and micro-satellites show the same engine mass fraction for altitudes up to about 250 km; this phenomenon may be due to a common ballistic coefficient. The engine mass fraction is the lowest for the nano-satellite, which may be due to its lower drag coefficient (sphere vs. flat plate) and higher ballistic coefficient (i.e., greater ability to penetrate the atmosphere). Fig. 8 shows that FEPT propulsion is not feasible for drag compensation at low altitudes. FEPT propulsion mass becomes a significant portion of the total spacecraft mass for altitudes below 150 km, and the entire spacecraft mass must be devoted to engine mass for an altitude range of 120-130 km. Finally, note that an extremely small fraction of total spacecraft mass must be devoted to FEPT engines for micro-satellites at altitudes above 300 km.

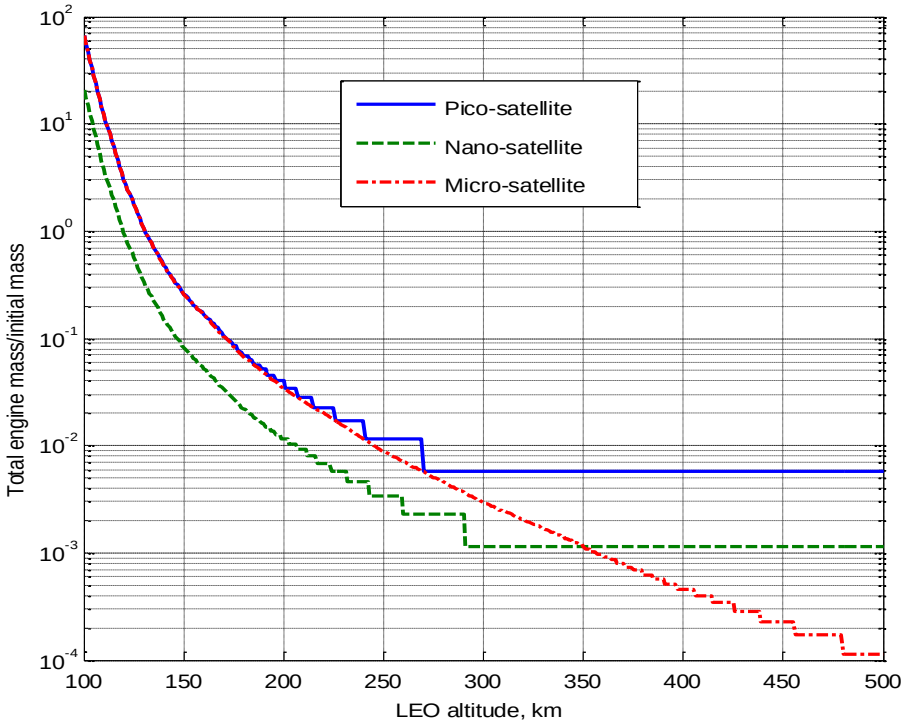

Figure 7. FEPT engine mass fraction required for drag compensation.

Fig. 8 shows the total FEPT engine-on time for the various satellites and altitudes. Total engine-on time is determined by dividing the total propellant mass by the total FEPT mass-flow rate, which is computed by multiplying the individual mass-flow rate of a single FEPT by the required number of engines. Total propellant mass is assumed to be 10% of the initial wet mass of the satellite. It is interesting that the pico- and micro-satellites show the same total engine-on time for altitudes up to about 250 km. Over 100 days of thrusting can be achieved before depleting all propellant for nano- and micro-satellites with altitudes greater than 225 km and 270 km, respectively. Pico- and nano-satellites have limited lifetimes of 100 days and 500 days for performing drag compensation even at high altitudes, while micro-satellites show very long lifetimes (3-11 yrs) for high altitudes.

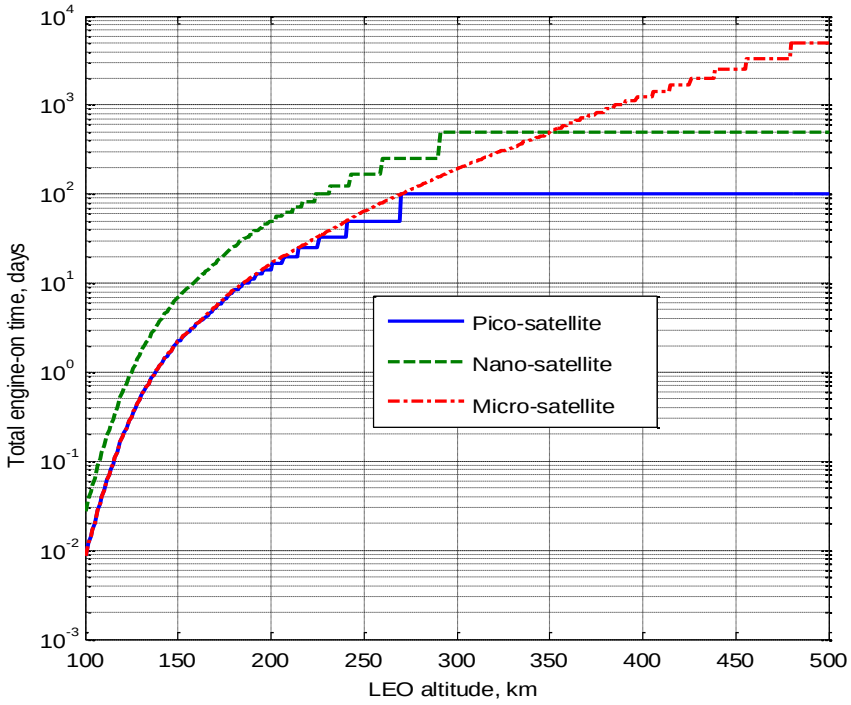

Figure 8. Total engine-on time required for drag compensation with a 10% propellant mass fraction.

B. On-Orbit Maneuvers

One potential application of the FEPT is primary propulsion for a very small autonomous inspection satellite, such as the Mini AERCam. The proposed Mini AERCam system has a total mass of 5 kg, and uses 12 cold-gas thrusters to maneuver.

We can compare the total potential velocity increment (ΔV) for on-orbit maneuvers for a typical cold-gas (nitrogen) thruster with the current FEPT design. Total propellant mass is assumed to be 0.5 kg for a nano-satellite system similar to Mini AERCam, or 10% of the initial spacecraft mass. Velocity increment is computed using the rocket equation

$$\Delta V = -gI_{sp} \ln(m_f / m_0) \tag{3}$$

where the final-to-initial mass ratio is 0.9. We assume that the cold-gas (N_2) system has an I_{sp} of 68 sec. A nano-satellite propelled by FEPTs has a total potential ΔV of about 620 m/s, while the cold-gas system can only provide a total potential ΔV of about 70 m/s.

IV. Conclusion

A ferroelectric plasma thruster is being developed at the University of Missouri for microspacecraft applications. It was determined that adding solid propellant material in the aperture of the device increases the emitted ion current from the FEPT. In addition, mission analysis was performed to determine the feasibility of using FEPTs for on-orbit maneuvers (such as drag compensation) for a range of miniature satellite classes.

Acknowledgments

This work was supported by the Air Force Office of Scientific Research.

References

[1] Mueller, J., Thruster Options for Microspacecraft: A Review and Evaluation of Existing Hardware and Emerging Technologies, *in AIAA/ASME/SAE/ASEE Joint Propulsion Conference and Exhibit*, 1997, pp. 97–3058.

[2] Gundel, H., Riege, H., Wilson, E., Handerek, J., and Zioutas, K., Fast polarization changes in ferroelectrics and their application in accelerators, *Nuclear Instruments and Methods in Physics Research Section A: Accelerators, Spectrometers, Detectors and Associated Equipment*, Vol. 280, No. 1, 1989, pp. 1 – 6.

[3] Rosenman, G., Shur, D., Krasik, Y. E., and Dunaevsky, A., Electron emission from ferroelectrics, *Journal of Applied Physics*, Vol. 88, No. 11, 2000, pp. 6109–6161.

[4] Puchkarev, V. F. and Mesyats, G. A., On the mechanism of emission from the ferroelectric ceramic cathode, *Journal of Applied Physics*, Vol. 78, No. 9, 1995, pp. 5633–5637.

[5] Dunaevsky, A., Krasik, Y. E., Felsteiner, J., and Dorfman, S., Electron/ion emission from the plasma formed on the surface of ferroelectrics. I. Studies of plasma parameters without applying an extracting voltage, *Journal of Applied Physics*, Vol. 85, No. 12, 1999, pp. 8464–8473.

[6] Kovaleski, S. D., Ion acceleration in a radio frequency driven ferroelectric plasma source, Vol. 33, No. 2, 2005, pp. 876–881.

[7] Kemp, M. A. and Kovaleski, S. D., "Thrust Measurements of the Ferroelectric Plasma Thruster," *Plasma Science, IEEE Transactions on* , vol.36, no.2, pp.356-362, April 2008

[8] Kemp, M. A. and Kovaleski, S. D., Ferroelectric plasma thruster for microspacecraft propulsion, *Journal of Applied Physics*, Vol. 100, No. 11, 2006, pp. 113306.

[9] David, L., "Military Micro-Sat Explores Inspection, Servicing Technologies," http://www.space.com/businesstechnology/050722_XSS-11_test.html, July 22, 2005.

[10] Fredrickson, S.E., Duran, S., and Mitchell, J.D., "Mini AERCam Inspection Robot for Human Space Missions," AIAA Paper 2004-5843, Space 2004 Conference and Exhibit, San Diego, CA, Sept. 2004.

[11] Lan, W., Brown, J., Toorian, A., Coelho, R., Brooks, L., Suari, J.-P., and Twiggs, R., "CubeSat Development in Education and into Industry," AIAA Paper 2006-7296, San Jose, CA., Sept. 2006.

[12] Harris, I, and Priester, W., "Theoretical Models for the Solar Cycle Variations of the Upper Atmosphere," *Journal of Geophysical Research*, Vol. 67, No. 12, 1962, pp. 4585-4591.